Mechanical Properties and Fracture Behavior of Blends of Acrylonitrile–Butadiene–Styrene Copolymer and Crystalline Engineering Plastics

Xiaodong Liu,[1] Antal Boldizar,[1] Mikael Rigdahl,[1] Hand Bertilsson[2]

[1]*Department of Polymeric Materials, Chalmers University of Technology, SE-412 96 Göteborg, Sweden*
[2]*Artimplant AB, Hulda Mellgrens gata 5, SE-412 32 Västra Frölunda, Sweden*

Received 27 April 2001; accepted 28 July 2001

ABSTRACT: The aim of this investigation was to evaluate the possibility of mechanically recycling blends of ABS with minor amounts of semicrystalline engineering plastics, such as polyamide, poly(ethylene terephthalate), and poly(butylene terephthalate). Compatibilizers and a core–shell impact modifier were incorporated into the blends in order to improve the mechanical properties. The toughness values, measured by the *J*-integral method, and the Charpy impact strength did not always exhibit consistent results, due to the significant difference in deformation rate and in fracture mechanism. The formation of co-continuous structures in the blends were noted and discussed. The fibrillation in the fracture surface contributed to the toughness as measured by the *J*-integral method. © 2002 Wiley Periodicals, Inc. J Appl Polym Sci 86: 2435–2448, 2002

Key words: blends; compatibilization; co-continuous; *J* integral; morphology; recycling

INTRODUCTION

Acrylonitrile–butadiene–styrene copolymer (ABS) is an amorphous styrene–acrylonitrile thermoplastic copolymer (SAN) with a grafted rubbery phase. It is the most commonly used engineering thermoplastic because of its competitive price. Due to its chemically bonded rubbery phase, it exhibits a reliable toughness even at low temperatures and with a sharp prenotch. Semicrystalline engineering plastics (designated XP), such as polyamide (PA), poly(butylene terephthalate) (PBT), and poly(ethylene terephthalate) (PET), have good chemical resistance and good abrasion resistance. Blends of ABS/XP can probably combine the good features from both the components and blends of these kinds have been studied earlier.[1–18] The aim of this work was to evaluate the possibilities of upgrading ABS-containing recycled engineering plastics by preparing ABS/XP blends. Since ABS is widely used, it is often the major component in the recycled engineering plastics. All the blends in this work were thus produced with ABS as the major component.

There are commercially available ABS/XP blends, such as Triax 1000 (ABS/PA, Bayer), Triax 4000 (ABS/PBT, Bayer), and Cycolin (ABS/PBT, GE). More details can be found in the comprehensive review of commercial blends by Utracki.[19] However, ABS and PA are not compatible. Neither ABS and PET nor ABS and PBT are miscible, but they have a limited affinity for each other. Therefore several compatibilizers are employed. These often contain functional acid, anhydride, or epoxide groups. Most of the previous investigations have aimed at toughening the XP phase with minor amounts of high impact ABS (high rubber content). In this work, a low-rubber-content, medium-impact-strength ABS was used as the major phase and XP as the minor phase. In order to increase further the toughness of the blends, a core–shell impact modifier was added in some cases.

In connection with mechanical recycling of polymers, it is of vital importance to characterize the mechanical properties, especially the toughness. Linear elastic fracture mechanics (LEFM) has been used to characterize the fracture behavior of brittle materials. In order for LEFM to be applicable, the deformation zone at the crack tip should be small. The crack starts to grow in an unstable manner when the stress intensity factor exceeds the critical value K_C. In other words, the crack initiates and then propagates (since the crack is unstable in brittle material) when the critical energy release rate G_C equals the fracture resistance R. For plastic materials, there is a larger plastic deformation zone at the crack tip and LEFM is not then suitable. The *J*-integral method is considered to be more appropriate in such a case. During the loading step of the *J*-integral evaluation, the potential energy of the specimen increases with increasing load, especially around the tip of the prenotch. The crack initiates from the prenotch when the energy required

Correspondence to: Mikael Rigdahl (rigdahl@polym.chalmers.se).

Contract grant sponsor: Foundation for Strategic Environmental Research (MISTRA).

TABLE I
Summary of the Engineering Plastics Used

Material	Trade Name	Density (kg/m^3)	Shear viscosity (Pa.s) (250°C) at 1000 s^{-1}	Shear viscosity (Pa.s) (250°C) at 100 s^{-1}	T_m (°C)	Supplier
PA6 B3	Ultramide B3	1130	140	250	220	BASF
PA6 B4	Ultramide B4	1130	700	1300	220	BASF
ABS	Commercial grade	1050	140	500	—	—
PBT	Ultradur B4520	1300	210	370	223	BASF
PET	Cleartuf P76	1385	—	—	250	Shell
PC	Makrolon 2800	1200	—	—	—	Bayer
SAN25	Commercial grade	1030	130	500	—	—

to create new fracture surface equals the associated decrease in potential energy of the specimen. In a ductile material, a stable or semistable crack propagates with further increase of the load. Analogous to the critical K_C value for LEFM, the critical J value can be evaluated in different ways in order to describe the energy required for crack initiation. Huang[20] pointed out that the shape of the corresponding crack resistance curve (J-R curve) gave a more comprehensive description of the fracture behavior. Since the cracks in many plastic materials propagate in a stable or semistable manner, not only the crack initiation energy but also the crack propagation energy is important for describing the fracture behavior. In order to make the crack propagate in a controlled manner, most of the J-integral measurements are performed at a low deformation rate.

Notched Charpy impact strength provides a very convenient, widely used, practical measure in which no attempt is made to separate the crack initiation and propagation steps.[21] The measured value has no clear physical meaning but is a rough estimate of the toughness at a high deformation rate (several m/s). The result depends strongly on the geometry, and especially on the tip radius of the prenotch. However, a high deformation rate is one of the most critical situations that a material may encounter. During high-speed fracture, heat is generated and dissipated at the crack tip as the crack propagates. The fracture surface is quite different from that obtained at a low deformation rate. In contrast to the Charpy impact strength measurement, the J-integral method can separate the crack initiation and crack propagation steps. It offers a better understanding of the fracture behavior of a material at a low deformation rate.

In this work, blends of ABS with PA, with PET or with PBT often exhibited a co-continuous structure to some extent. The fracture behavior can be affected by the appearance of such a structure. Fibrillar structures in a three-point-bend fracture surface obtained at a low deformation rate have earlier been reported for ABS/PA6 blends with styrene–maleic anhydride copolymers as compatibilizers.[1] The fibrillar structure can be related to the enhanced slow crack propagation resistance of the material as shown by the J-R curve or the critical crack initiation energy J_C. The styrene–maleic anhydride functional copolymers can react with the amine end groups in polyamide chains and produce a block copolymer with styrene–maleic anhydride blocks and polyamide blocks, and such a emulsifier thus reduces the interfacial tension between SAN (styrene–acrylonitrile copolymer) and PA. The previously used styrene copolymers contained 8 or 14% maleic anhydride (SMA8 or SMA14), and they were not optimal compatibilizers since they were not completely miscible with the matrix of ABS used here, i.e., SAN with 25% acrylonitrile.[2] Increasing the maleic anhydride content to 25% gives a compatibilizer (SMA25) that is completely miscible with this SAN matrix. The efficiency of SMA25 as compatibilizer was investigated in this study. Other compatibilizers with epoxy functional groups and without any functional groups were also evaluated to some extent. In addition to the toughness evaluation, the tensile properties of the blends, such as yield strength, elongation at break, and tensile modulus, were also determined. Furthermore, we continued to investigate the mechanism of generation of the fibrillar structures obtained at a low deformation rate.

MATERIALS

Some properties of the engineering plastics used are summarized in Tables I and II. The matrix of the ABS material, SAN, contained 25% acrylonitrile. A styrene–acrylonitrile copolymer with 25% acrylonitrile (SAN25) was used to compare the morphologies of the ABS/PA and the SAN25/PA blends.

Two kinds of styrene–maleic anhydride copolymer (SMA) were used as reactive compatibilizers. SMA14 is a polystyrene copolymerized with 14% maleic anhydride. It is in the margin of the miscibility window for SAN and SMA. SMA25 is a copolymer of styrene with 25% maleic anhydride, and it is fully miscible with the SAN25 matrix. Both SMAs can react with amine or hydroxyl groups at the processing temperature used. Polycarbonate (PC) was used as compatibilizer for the ABS/polyester blends. EXL3300 used in the ABS/XP blends (Paraloid EXL 3300 from Rohm & Haas) was an all-acrylic core–shell impact modifier in

TABLE II
Mechanical Properties of the Materials Used

Materials	Tensile Modulus (GPa)	Yield Strength (MPa)	Elongation at Break (%)	Impact Strength Notched (kJ/m^2)	J_C (kJ/m^2)
ABS	2.3	40	14	13.0	8.9
PA6 B3	2.3	63	>150	13.8	—
PA6 B4	2.3	65	>150	15.0	—
PBT	2.5	60	>50	6.0	—
PET (amorphous state)	2.3	50	>270	5.7	—

the form of granules consisting of particles with a diameter of 0.3 μm. The particles consist of a polymethylmethacrylate (PMMA) shell and an acrylic rubber core.

The epoxide-containing compatibilizer used in the ABS/PA and ABS/PET blends was produced in our laboratory using PMMA, glycidyl methacrylate (GMA) monomer, and dicumyl peroxide (DCP) initiator. The PMMA (Plexiglas 6N from Rohm & Haas) was functionalized with the GMA–monomer during reactive extrusion. The GMA (purity 97%, used as received) monomer was purchased from Sigma-Aldrich. The DCP initiator (purity 98 %, half-life time 12 s at 190°C) was also a product from Sigma-Aldrich.

EXPERIMENTAL

Functionalization of PMMA with GMA

A liquid mixture of GMA and 2% DCP was added dropwise into the hopper of a twin-screw extruder (Werner & Pfleiderer ZSK 30 M 9/2) while PMMA pellets were fed in. The GMA mixture/PMMA ratio was 8/92 (by weight). The barrel temperature was 210°C, and the rotational speed of the screw 170 rpm. The extrudate was the graft copolymer poly(methyl methacrylate-co-glycidyl methacrylate) (designated PMMA-GMA).*

Twin-screw extrusion and injection molding

In order to obtain specimens for the mechanical tests, blends were produced in the twin-screw extruder at a processing temperature of 250°C (except for PET-containing blends, for which the processing temperature was 270°C) and with a screw speed of 200 rpm. The extrudates were pelletized with a granulator. Test specimens were injection molded in an Engel 330/80 injection molding machine at melt and mold temperatures of 250°C (270°C for PET blends) and 50°C, respectively.

Measurements of the mechanical properties

The mechanical properties were determined at a temperature of 22 $\pm$ 1°C and a relative humidity of 55 $<$ 10%. All the specimens were conditioned for 24 h before testing. The yield strength, tensile modulus, and elongation at break were measured in accordance with ISO527-2 standard, at a crosshead speed of 5 mm/min (strain rate 0.0014 s^{-1}) with a Zwick UTM 1455. The average values of at least 5 specimens are reported. The Charpy impact strength was determined using a Frank KMO 79 impact tester, according to ISO 179 standard specimen type 2. The average values of at least 10 specimens are reported. The typical deviations are less than 10% for tensile modulus and yield strength values, and less than 30% for elongation at break and impact strength values.

The *J*-integral evaluation was performed using a three-point-bend fixture in a tensile testing machine, Instron Model 1193, at a crosshead speed of 2 mm/min, in accordance with the ASTM standards D6086-96 and formerly E813-89. The details of this method are described elsewhere.[1] The crack resistance curve was described using a power law function:

$$J = C_1(\Delta a)^{C_2} \quad (1)$$

where C_1 and C_2 describe the shape of crack resistance curve, and Δa is the slow crack propagation length. J_c is the critical J value defined by ASTM E813-89 and this value is taken as the crack initiation energy.

Scanning electron microscopy (SEM)

The structure of the specimens was investigated using a Digital Scanning Electron Microscope Zeiss DSM 940A. The surfaces were coated with a thin gold layer, about 50 Å thick.

An etching technique was used to remove the SAN phase in order to reveal the morphology of the blends. Acetone, which is a solvent for the SAN phase of ABS

*When carrying through the experiment in other ways than described here, risk of harm or injury might exist. Adequate level of safety, use of proper safety equipment, and competent handling are also required in order to eliminate possible risks.

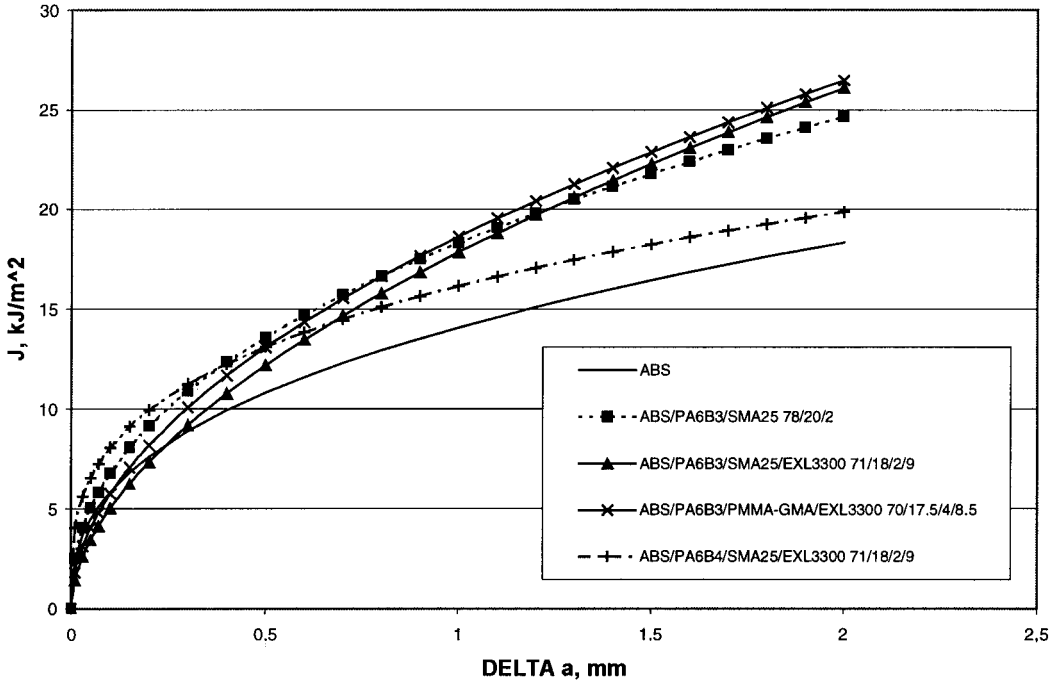

Figure 1 Crack resistance curve of ABS/PA blends. (The points are not real data values, but only used to distinguish the curves.)

but a nonsolvent for PA, PET, or PBT, was used for this purpose. The sample was cut to expose a surface parallel to the flow direction in the middle of the injection-molded tensile-test bar.

RESULTS AND DISCUSSION

Mechanical properties

ABS/PA blends

Since the simple, incompatible blend of ABS and PA exhibited a rather poor mechanical behavior, SMA25 and EXL3300 rubber were used as compatibilizer and impact modifier, respectively. SMA25 is fully miscible with SAN25,[2] which is the matrix of the ABS. Table 3 summarises the mechanical properties of the ABS/PA blends. The ABS/PA6 B3 78/20 blend (weight fraction in %) with 2% SMA25 compatibilizer exhibited a higher tensile modulus, yield strength, and elongation at break than the pure ABS (Table II). The mechanical properties of PA are known to be sensitive to moisture and PA6 B3 has a high modulus and yield strength at a low moisture content. It was thought that the blending of ABS and PA might possibly reduce the moisture absorption in the PA phase, and thereby promote a higher modulus and higher yield strength. However, the Charpy impact strength of the blend was only 6.5 kJ/m^2, i.e., much lower than the value of 13.0 kJ/m^2 for pristine ABS. In contrast to the impact tests, the *J*-integral measurements revealed another trend. The J_C value of this blend was higher than that of ABS. The *J-R* curve (Fig. 1) also shows that the energy absorption during slow crack propagation was higher for the blend than for ABS.

With 9% EXL3300 core–shell impact modifier, the elongation at break of the blend ABS/PA6 B3/SMA25 was not substantially higher than that of the blend without EXL3300. The Charpy impact strength, however, increased to 13.5 kJ/m^2 with the impact modifier, which was a significant improvement over the blends without this additive. This indicates that EXL3300 can be an important additive for retaining the impact strength of a ABS/PA6 blend. The J_C value for the blend was slightly higher than that of ABS and the *J-R* curve was above the corresponding curve for ABS, except at the beginning of the crack propagation (see Fig. 1).

The blend of ABS with the higher molecular weight PA6 B4, i.e., ABS/PA6 B4 71/18 blend with 2% SMA25 and 9% EXL3300 also exhibited good mechanical properties (see Table III). The elongation at break was greater than 90%, i.e., significantly higher than that of the similar blend with PA6 B3. The J_C value was lower for the latter blend, although both blends had similar Charpy impact strengths. As shown in the next section, the ABS/PA6 B3/SMA25 blends formed thinner and shorter fibrils during slow crack propagation. The PMMA shell of EXL3300 is miscible with the SAN phase of ABS, but it is not compatible with polyamide. SMA25 can, however, act as compatibilizer for EXL3300 and PA6, due to its miscibility with the PMMA-shell and its reaction with PA.[22] However, the toughness values measured at low deformation rates, such as the elongation at break and *J*-integral values,

TABLE III
Mechanical Properties of ABS/PA Blends

Composition	Tensile Modulus (GPa)	Yield Strength (MPa)	Elongation at Break (%)	Impact Strength Notched (kJ/m^2)	J_C (kJ/m^2)
ABS/PA6 B3/SMA25 78/20/2	2.5	49	27	6.5	11.1
ABS/PA6 B3/SMA25/EXL3300 71/18/2/9	2.2	43	32	13.5	9.3
ABS/PA6 B3/PMMA-GMA/EXL3300 70/17.5/4/8.5	2.0	38.7	47	10.6	10.7
ABS/PA6 B4/SMA14 77/20/3	2.3	44	11	5.0	N/A
ABS/PA6 B4/SMA25/EXL 3300 71/18/2/9	2.0	39	>90	13.9	11.7

were not greatly influenced by the impact modifier compared with the value for the blend of ABS/PA6 B3/SMA25. The ABS/PA6 B4 /SMA14 77/20/3 blend did not exhibit particularly good mechanical properties since SMA14 was not an adequate compatibilizer for the ABS/PA blend.

The reason for using PMMA-GMA as a compatibilizer was to compare the efficiency of this polymer with that of SMA25. PMMA is miscible with the SAN matrix of ABS and the epoxy functional groups are capable of reaction with the carboxylic acid and amine groups of the polyamide.[7] It should thus be able to act as a compatibilizer for the ABS/PA blends. The technique used also offers the possibility of creating a compatibilizer via free radical grafting in an extruder, and this thus provides a convenient method of introducing functional groups into an "inert" polymer. PA/ABS/PMMA-GMA blends have been previously investigated by Paul et al.[7] However, the PMMA-GMA in their work was synthesized in a flask by solution polymerization. PA was the major component of the blends and high rubber content ABS was incorporated as toughening agent.

In the present work, the blend of ABS/PA B3 70/17.5 with 4% compatibilizer PMMA-GMA and 8.5% impact modifier EXL 3300 had a notched Charpy impact strength of 10.6 kJ/m^2, which is lower than the value of 13.5 kJ/m^2 observed for the similar blend but with SMA25 as compatibilizer. The elongation at break was 47%, i.e., higher than the 32% recorded for the SMA25-compatibilized blend. The J_C value of the PMMA-GMA-compatibilized blend was slightly higher than that of the SMA25-compatibilized blend and the same trend was also revealed by the *J-R* curve. This difference in toughness characteristics can be attributed to the different fracture behaviors of the two blends. The PMMA-GMA-containing blends exhibited thicker and much longer fibrils in the low deformation rate fracture surface, which might be the reason for the somewhat higher slow deformation toughness. However, in view of the Charpy impact results, it is probable that that SMA25 should be regarded as a more efficient compatibilizer than PMMA-GMA for overall toughness.

ABS/PBT blends

By analogy with PC/SAN blends, SAN and thermoplastic polyesters exhibit some interaction with each other. However, such an interaction is insufficient by far to establish a stable morphology.[9–12] As shown in Table IV, the binary blend of ABS/PBT 67/33 exhibited mechanical properties comparable with those of pure ABS, which indicates some degree of compatibility between the two components. Small amounts of SMA25 were incorporated to enhance the interfacial strength via the miscibility with SAN25. SMA25 is also capable of reacting with the hydroxyl groups of polyesters. The ABS/PBT 61/26 blend with 4% SMA25 and 9% EXL3300 impact modifier had better mechanical properties than ABS, as shown in Table IV. Two functions were expected from SMA25. First, it can improve the interfacial affinity between ABS and PBT by *in situ* compatibilization. Second, the PMMA shell of EXL3300 is not compatible with PBT, whereas SMA25 is mutually miscible with PMMA and capable of reaction with PBT. SMA25 can therefore promote the dispersion of EXL3300 in the PBT phase.

The use of 9% PC instead of 4% SMA25 (ABS/PBT/PC/EXL3300 55/27/9/9) leads to similar mechanical

TABLE IV
Mechanical Properties of ABS/PBT Blends

Composition	Tensile Modulus (GPa)	Yield Strength (MPa)	Elongation at Break (%)	Impact Strength Notched (kJ/m^2)	J_C (kJ/m^2)
ABS/PBT 67/33	2.3	46	15	9.9	7.6
ABS/PBT/PC/EXL3300 55/27/9/9	2.1	43	34	16.9	11.6
ABS/PBT/SMA25/EXL3300 61/26/4/9	2.2	43	23	16.6	9.5

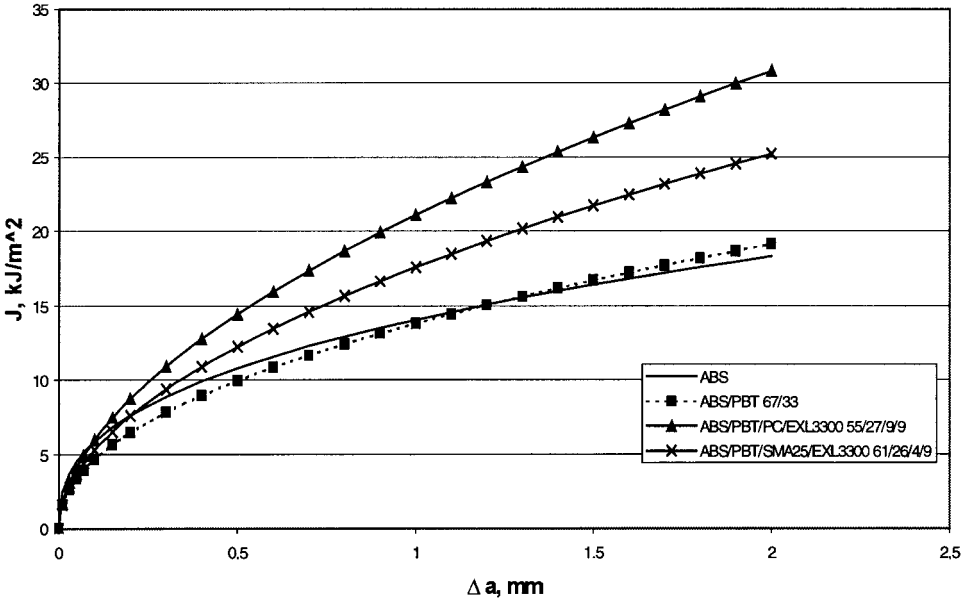

Figure 2 Crack resistance curve of ABS/PBT blends.

properties (cf. Table IV). The role of PC is much the same as that of SMA25. It improves the interfacial affinity between the ABS and PBT phases, since PC is compatible with both SAN and PBT. PC is also almost miscible with PMMA, which means that it can improve the dispersion of EXL3300 in the PBT phase. Moreover, unlike the brittle SMA25, polycarbonate has a substantial inherent toughness. Since PBT/PC is a frequently used commercial blend, this combination should be of interest in practice. As shown in Table IV and Figure 2, the mechanical properties, such as the tensile properties, the Charpy impact strength, and the J_C values, of the two ABS/PBT blends with the core–shell impact modifier and the compatibilizers, were better than those of ABS. For these two blends, the Charpy impact strength and *J*-integral measurements show consistent results, i.e., both methods gave high values for the blends.

ABS/PET blends

The miscibility of SAN and PET is poorer than for the PBT/SAN blend. As a result, the blends of ABS with PET had an impact resistance inferior to that of the ABS/PBT blends. The Charpy impact strength of ABS/PET 67/33 was actually only one quarter of that of ABS, as shown in Table V. On the other hand, the *J*-integral measurements did not indicate any great difference with regard to toughness between these two materials at a low deformation rate. Using PC as compatibilizer, the elongation at break of the ABS/PET/PC 60/30/10 blend surprisingly dropped to 4.2%, whereas the other mechanical properties were largely unaffected. The incorporation of 9% EXL3300 core–shell impact modifier into the system increased the elongation at break to >150%. The Charpy impact strength was improved to 7.0 kJ/m^2, more than double that of the ABS/PET 67/33 and the ABS/PET/PC 60/30/10 blends. The use of SMA25 or PMMA-GMA as compatibilizer gave blends with a slightly lower ultimate strain than that noted for ABS. The blend with 4% SMA25 had only half the Charpy impact strength of the ABS. However, the *J*-integral measurements gave J_C values and *J-R* curves (Fig. 3) quite close to those of ABS. The similar blend with PMMA-GMA as compatibilizer, i.e., the ABS/PET/PMMA-GMA/

TABLE V
Mechanical Properties of ABS/PET Blends

Composition	Tensile Modulus (GPa)	Yield Strength (MPa)	Elongation at Break (%)	Impact Strength Notched (kJ/m^2)	J_C (kJ/m^2)
ABS/PET 67/33	2.4	49	13	2.9	8.0
ABS/PET/PC 60/30/10	2.4	51	4.2	3.3	9.1
ABS/PET/PC/EXL3300 55/27/9/9	2.2	46	>150	7.0	11.0
ABS/PET/SMA25/EXL3300 61/27/3/9	2.2	49	9.4	7.3	9.1
ABS/PET/PMMA-GMA/EXL3300 61/26/4/9	2.1	46	9.8	7.9	7.4

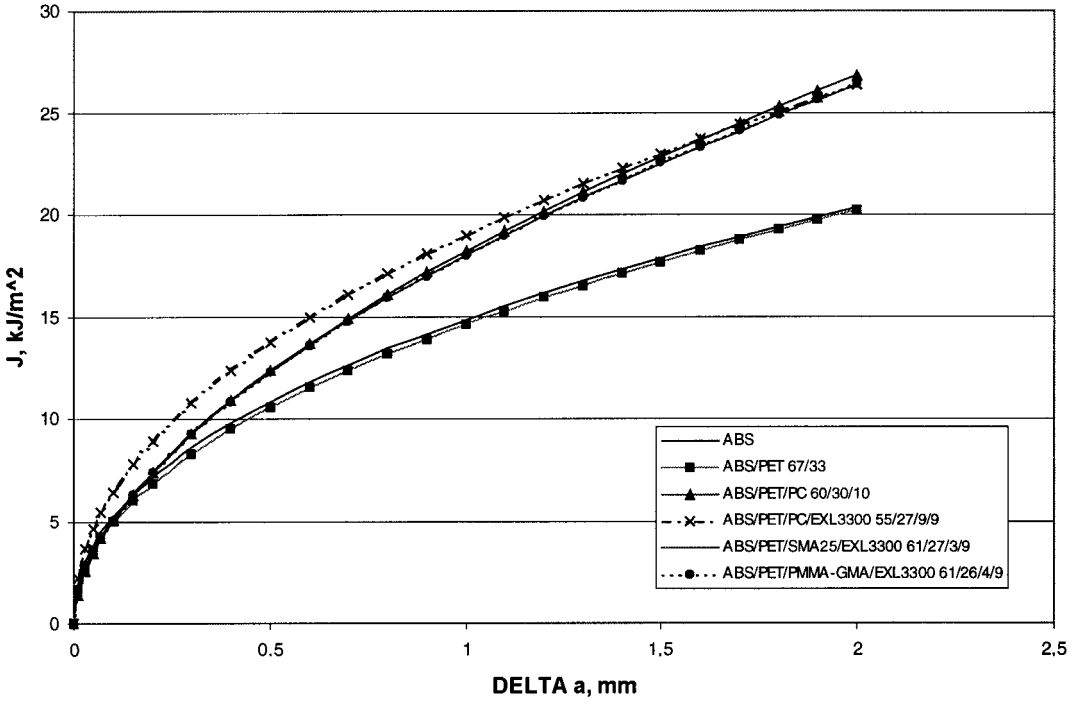

Figure 3 Crack resistance curve of ABS/PBT blends.

EXL3300 61/26/4/9 blend, exhibited the same *J-R* curve as the SMA25-compatibilized blend (see Fig. 3).

Morphology

Acetone-etched surfaces of injection-molded ABS/XP blends

The XP-phase morphology of the blends before the mechanical testing was examined using etching. The SAN phase of ABS in the blends was dissolved in acetone and the etched surface then showed the structure of the XP phase. The blends of ABS/PA6 B3 78/20 with 2% SMA25 and the same composition blend plus 9% EXL3300 both exhibited a continuous PA phase in the acetone-etched surface. The dimension of the PA phase in the direction perpendicular to the flow was 1–2 μm, as shown in Figures 4(a) and 4(b). PA6 B4 had a shear viscosity about four times higher than PA6 B3 at 1000 s^{-1} and 250°C, but it also formed a continuous structure in the blend with ABS, as shown in Figures 4(c) and 4(d). In accordance with the complicated composition of some of the blends, the etched surface also exhibited a complicated morphology, e.g., small particles were observed in blends with the EXL3300 core–shell impact modifier. Similar continuous structures were also observed in the ABS/PET and the ABS/PBT blends; one example of an ABS/PET 55/27 blend with 9% of PC and 9% EXL 3300 is shown in Figure 5. The EXL3300-rubber particles are not, however, very distinct in this micrograph. A possible reason is that EXL 3300 did not adhere to the PET phase, since no reactive compatibilizer was used in this blend.

The formation of the co-continuous structure

The morphology or structure of a polymer blend is assumed to be governed by a number of factors, such as the viscosity ratio between the two components, the corresponding volume ratio, and the interfacial tension. Two kinds of polyamides were used here to study the influence of the viscosity ratio between PA and ABS, the molecular mass, and the end group content of the PA phase on the morphology of the ABS/PA blends. The shear viscosity values are given in Table I. The shear rates in the twin-screw extruder and in the injection molding machine are assumed to be of the order of 100 and 1000 s^{-1}, respectively. During the compounding of the polymer blends, large droplets of one of the components deformed and decreased in dimension perpendicular to the flow direction and increased in the flow direction, resulting in fibrillation and a larger interfacial area. The interfacial tension tends, however, to decrease the interfacial area. As a result, the elongated threads may break down into small particles (the Raleigh disturbance). The driving forces for this disintegration are the viscosity ratio, the interfacial tension, and the dimensions of the threads.[23] However, the disintegration process may be inhibited or retarded, resulting in a co-continuous structure. Quite often, co-continuous structures are formed when the following rheological criterion is fulfilled[24]:

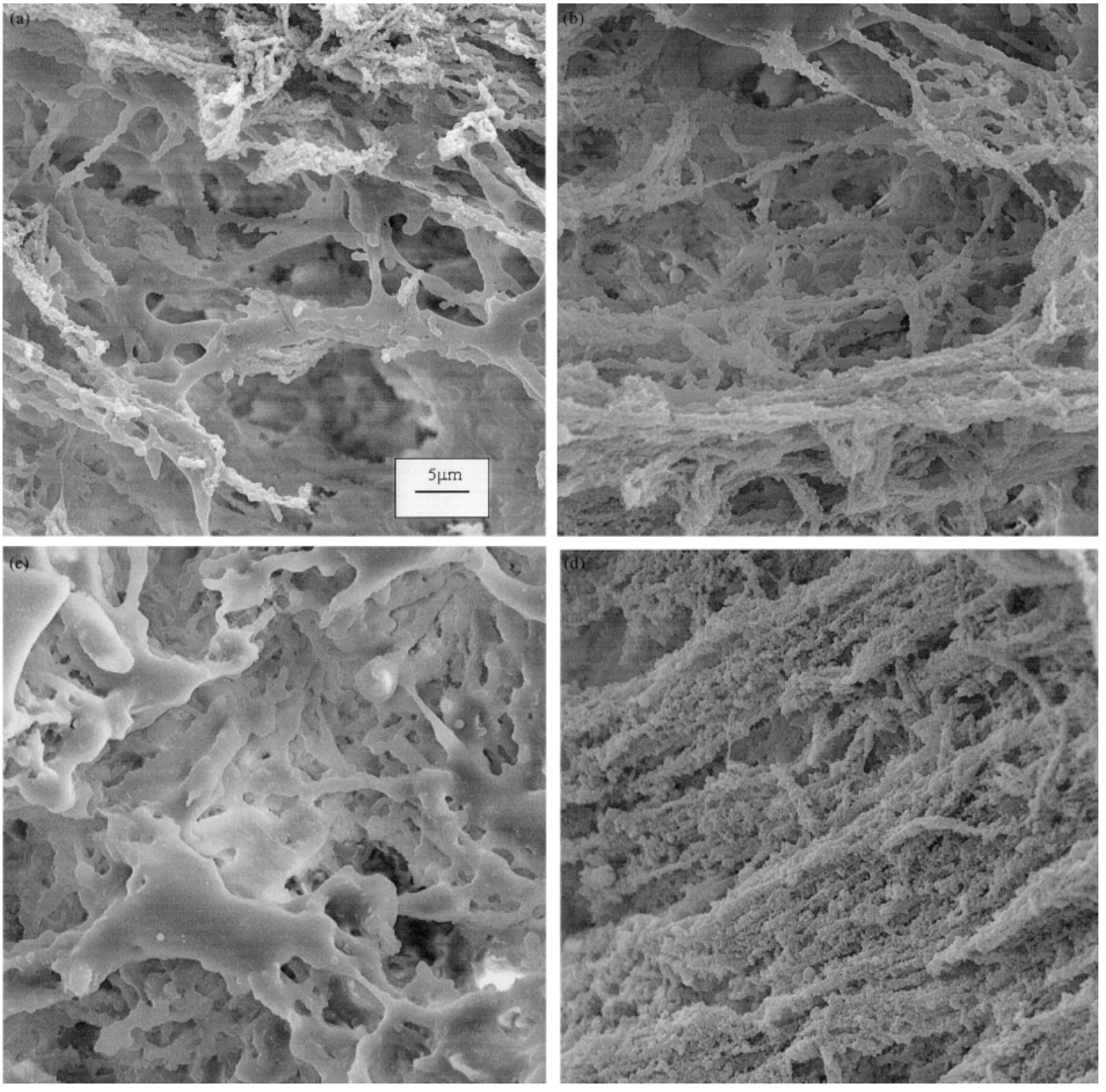

Figure 4 The ABS/PA6 blends morphology by acetone etching (magnification is the same in all these four micrographs). (a) ABS/PA6 B3/SMA25 78/20/2, (b) ABS/PA6 B3/SMA25/EXL3300 71/18/2/9, (c) ABS/PA6 B4/SMA14 77/20/3, and (d) ABS/PA6 B4/SMA25/EXL3300 71/18/2/9.

$$\frac{\eta_1}{\eta_2} \cdot \frac{\phi_2}{\phi_1} \approx 1 \qquad (2)$$

Here the η_i are the viscosities of the components at the processing conditions and ϕ_i are the corresponding volume fractions. Our previous experiments[1] showed, however, that the ABS/PA system did not satisfy this criterion. For instance, the ABS/PA6 B3 blend exhibited a co-continuous structure, as shown in Figure 4(a) and 4(b). The shear viscosity of ABS and PA6 B3 were the same at 1000 s^{-1}, but the volume ratio was about 0.8/0.2 since the melt densities of these two materials are very close. Equation (2) then gives a value of 4, far from unity.

The microrheology theory[24] of polymer blends can provide a description of the macroscopic rheological properties and of the phase structure of the multiphase system during flow. Some factors other than the viscosity ratio and the volume ratio may inhibit the disintegration process and thus stabilize the fibril structure.[23,24] The drop deformability and disintegration mechanisms are to some extent controlled by the capillary number κ, a dimensionless parameter given[23] by

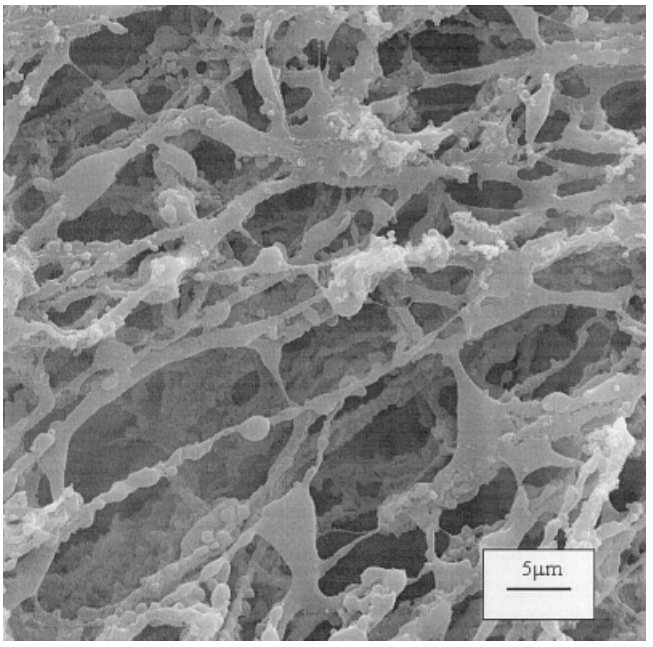

Figure 5 The acetone-etched surface of the ABS/PET/PC/EXL3300 55/27/9/9 blend.

$$\kappa \equiv \frac{\sigma * r}{\gamma} \tag{3}$$

where r is the local radius of the thread (or the particle), γ is the interfacial tension, and σ the stress applied to the thread (or the particle). The critical capillary number κ_{Cr}, which governs the droplet deformation and thread break-up process, also depends on the viscosity ratio and the type of flow (shear or elongational). For $0 < \kappa/\kappa_{Cr} < 0.1$, no droplet deformation takes place; for $0.1 < \kappa/\kappa_{Cr} < 1$, the droplet deforms but does not break; for $1 < \kappa/\kappa_{Cr} < 4$, the droplet deforms and breaks; and for $\kappa/\kappa_{Cr} > 4$, long and stable threads (fibrils) are formed. The κ_{Cr} value depends on the viscosity ratio under the shear flow conditions, but not during elongational flow, which can be of importance in the present situation. This discussion applies only to Newtonian liquids in simple flow, but it can provide a general description in the case of more complex systems. A more detailed discussion can be found in the literature.[24,25]

The mixing of ABS/XP melts is certainly a complex process. For example, during the reactive compatibilization, the viscosity of the PA phase increases somewhat as a result of the chemical reaction. Furthermore, the processing of a polymer often involves elongational flow, which can result in thread (or fibril) formation,[23,24] i.e., a kind of co-continuous structure. It has actually been reported that threads of polyamide can appear at a temperature as low as 69°C below its melting temperature in an elongational flow field.[24] Many crystalline engineering polymers tend to strain harden during elongation, i.e., the elongational viscosity increases with increasing strain rate. This counteracts the tendency towards thread or fibril break-up and leads to a certain degree of co-continuity. In addition, the interfacial tension, which is a driving force for thread break-up, can be reduced due to the presence of compatibilizers. Furthermore, the molecular weight of the interface region increases due to the reaction between the reactive compatibilizer and the respective polymer, and this rigidifies the interface and inhibits thread break-up. Another reason for the apparent co-continuous structure may be that the melting temperature of PA6 is 220°C, i.e., rather close to the processing temperature used. The same applies to PET and PBT, which have melting temperatures of 250°C (the processing temperature was 270°C) and 223°C, respectively. The co-continuous morphology generated under shear and elongational flow fields may therefore be frozen-in soon after the blends have left the processing zone. These phenomena can certainly contribute to the appearance of a co-continuous structure even though the requirements of eq. (2) may not be fulfilled.

As shown in Table I, SAN25 and ABS had the same shear viscosity level at a shear rate of 1000 and also at 100 s^{-1}, although the morphologies of the ABS/PA blends and the SAN/PA blends were quite different. The ABS/PA6 blends had a co-continuous appearance, whereas the SAN/PA6 blend exhibited a normal dispersed particle/matrix structure. A possible reason is that ABS, although displaying an overall high viscosity, had a lower viscosity SAN matrix, i.e., the rubber particles contributed significantly to the viscosity of the ABS polymer. In the ABS/XP blends, the XP component would then be surrounded by a low viscosity SAN. The stress field is therefore different from that in the SAN/PA blend.

The governing conditions for the co-continuous formation in ABS/PA blends are obviously not well understood. However, the above discussion indicates some factors that may be important in this context. Clearly, further studies are required in order to ascertain the relevant mechanisms involved.

The fibrillar morphology of fracture surfaces of *J*-integral specimens

A fibrillar morphology of the fracture surfaces of *J*-integral specimens has previously been observed for ABS/PA6B4 80/20 blends with SMA8 and SMA14 (styrene–maleic anhydride copolymers with 8 and 14% maleic anhydride, respectively) as compatibilizers.[1] The continuous PA phase does not instantly fracture together with the ABS during the slow crack propagation. Instead, it is pulled out from the ABS and deformed, leaving fibrils in the fracture surface.

The PA B3 melt had the same shear viscosity as ABS at the higher shear rate (Table I). The blend ABS/PA B3 78/20 with 2% SMA25, and the same blend plus 9%

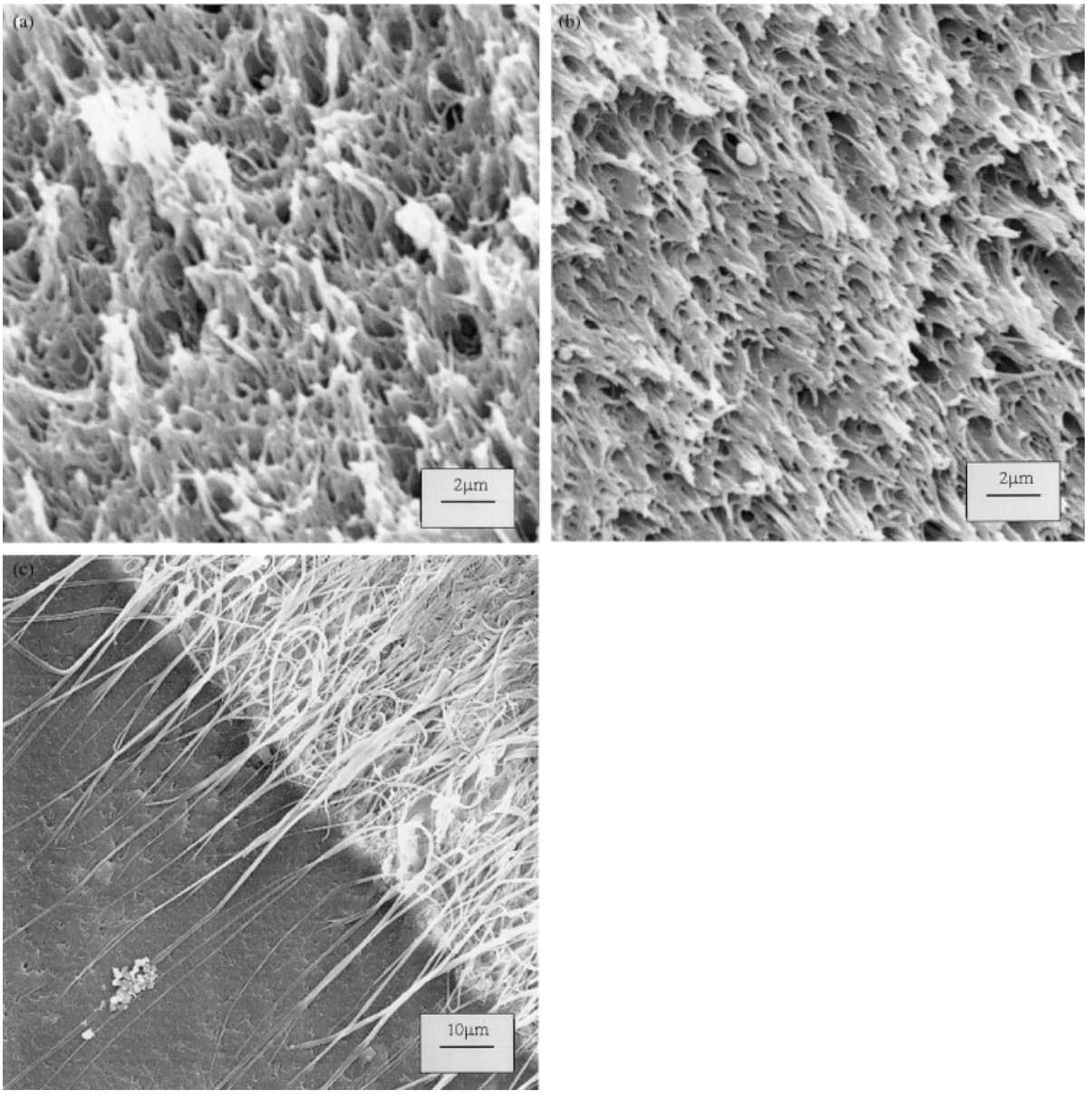

Figure 6 SEM micrographs of the fracture surface of *J*-integral specimen of ABS/PA6 B3 blends. (a) ABS/PA6 B3/SMA25 78/20/2, (b) ABS/PA6 B3/SMA25/EXL3300 71/18/2/9, and (c) ABS/PA6 B3/PMMA-GMA/EXL3300 70/17.5/4/8.5.

EXL3300 exhibited co-continuous structures in the etched surface. The corresponding *J*-integral fracture surfaces had fibrils in the slow crack propagation zone. The fibrils were tiny and not very long [see Fig. 6(a) and 6(b)]. The thicker PA6 B3 phase in Figure 4(a) in the undeformed ABS/PA6 blend and the thinner PA6 B3 phase in Figure 6(a) in the deformed blend imply that the fibrils were elongated from a thicker PA phase. For the blend containing PMMA-GMA as compatibilizer, the fibril structure was also found in the "slow fracture" surfaces. In this blend, the fibrils were thicker and very long, up to 200 μm [see Fig. 6(c)]. Such a difference indicates that the compatibilizer can influence the formation of the fibrils during fracture. The dark region in Figure 6(c) is the prenotch of the *J*-integral specimen.

The PA6 B4 melt had a significantly higher shear viscosity than ABS and PA6 B3 at shear rates of 100 and 1000 s^{-1}. The co-continuous structure also appeared in the etched surfaces of the corresponding ABS/PA6 B4 blends as previously mentioned. The ABS/PA6 B4 blends also showed fibril structures in the "slow fracture" surfaces [see Figs. 7(a) and 7(b)]. The ABS/PA6 B4 77/20 blend with 3% SMA14 had fibrils as well as some particles in the fracture surface of the *J*-integral specimens. The ABS/PA6 B4 71/18 blend with 2% SMA25 and 9% EXL3300 exhibited longer and thicker fibrils than those of the similar PA6 B3 blend. Such a difference indicates that the molecular weight (or viscosity) of the polyamide can influence the formation of the fibril structure.

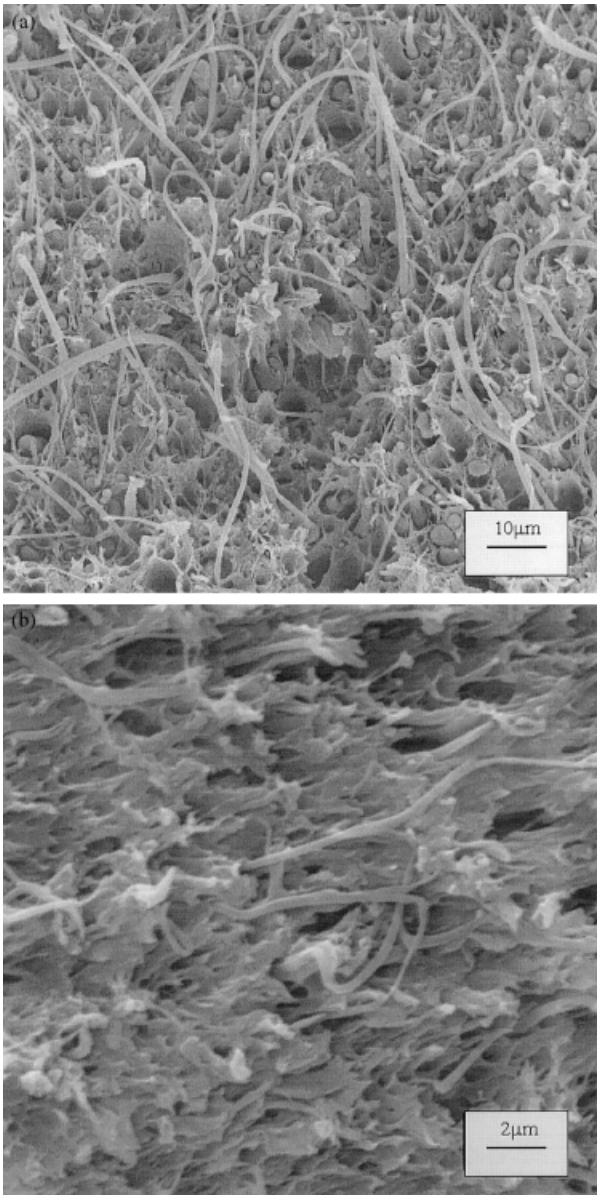

Figure 7 SEM micrographs of the fracture surface of *J*-integral specimens of ABS/PA6 B4 blends. (a) ABS/PA6 B4/SMA14 77/20/3 blend and (b) ABS/PA6 B4/SMA/EXL3300 71/18/2/9 blend.

The ABS/PET and ABS/PBT blends also exhibited co-continuous structures similar to those of the ABS/PA blends. The ABS/PET 67/33 blend contained short ribbon-like fibrils and rather poorly dispersed particles, as an indication that the PET was not very well dispersed in the ABS phase [Fig. 8(a)]. When 10% PC was added to the ABS/PET 60/30 blend, more finely dispersed fibrils were noted [see Fig. 8(b)]. This indicates that PC could reduce the interfacial tension between ABS and PET. However, as noted previously, the mechanical properties were not affected. The elongation at break value even dropped when PC was added. With the EXL3300 core–shell impact modifier, the fibril morphology did not change [see Figure 8(c)].

The dispersion of PBT in ABS was better than that of PET, i.e., the radii of the fibrils were smaller. However, ABS/PBT 67/33 blend also contained some thick fibrils, like "ribbons, the fibrils decreased dramatically with the addition of the compatibilizers. The fracture surfaces of the *J*-integral specimens are shown in Figures 9(b) and 9(c) for ABS/PBT/EXL3300 blends with 9% PC and 9% SMA25 as compatibilizers. The fibrils were very tiny, indicating a good dispersion of the PBT in the ABS. In the blend ABS/PBT/PC 50/25/25 with 9% of EXL3300, there were, however, no fibrils [see Fig. 9(d)]. This illustrates that the fibril structure appeared only with certain compositions.

To our knowledge, this kind of fibril structure in fracture surfaces has been reported for ABS/XP blends only once before.[26] However, similar fibril structures have been noted in other blend systems. It has been known for a numbers of years that some polymer blends exhibit co-continuous structures. The blend technique has actually been used to prepare ultrafine fibers for more than 30 years.[27,28] These microfibers are produced via melt spinning of the blend through a die followed by extraction of the matrix phase, which is normally water soluble. The key parameters involved are the interfacial tension between the polymer blend constituents, the composition ratio, and the viscosity ratio. Other blends that exhibit fibrillar structures in the fracture surfaces are blends of liquid crystalline polymers (LCP) with some conventional plastics. In the fracture surface or etched surface of such self-reinforced alloys, the LCP fibrils were clearly revealed.[29,30] However, such a morphology was formed mainly at the transition (solid to nematic transition) temperature. Extensional flow was essential for LCP fibrillation, although fibril formation was also possible in shear flow within a certain range of viscosity ratios.[29,30]

The mechanism of fibril formation and corresponding energy dissipation during slow crack propagation

The fibrils in the ABS/XP blends are believed to form according to the following. ABS and XP form a co-continuous structure during processing, as described in the previous section. There are also some XP particles in the blends, but they are not involved in the fibril formation during the slow deformation loading. In the *J*-integral measurements, a crack propagates slowly from the prenotch when a load is applied. A model picture of the fibril formation during the slow crack propagation is given in Figure 10. Ahead of the crack tip, there is plastic deformation, in both the ABS and XP phases, zone C. The ABS phase fractures upon further deformation, but the XP phase, which is more ductile, does not break but is further elongated. The fibrils are formed when the XP phase is pulled out from the ABS phase and the XP phase is deformed.

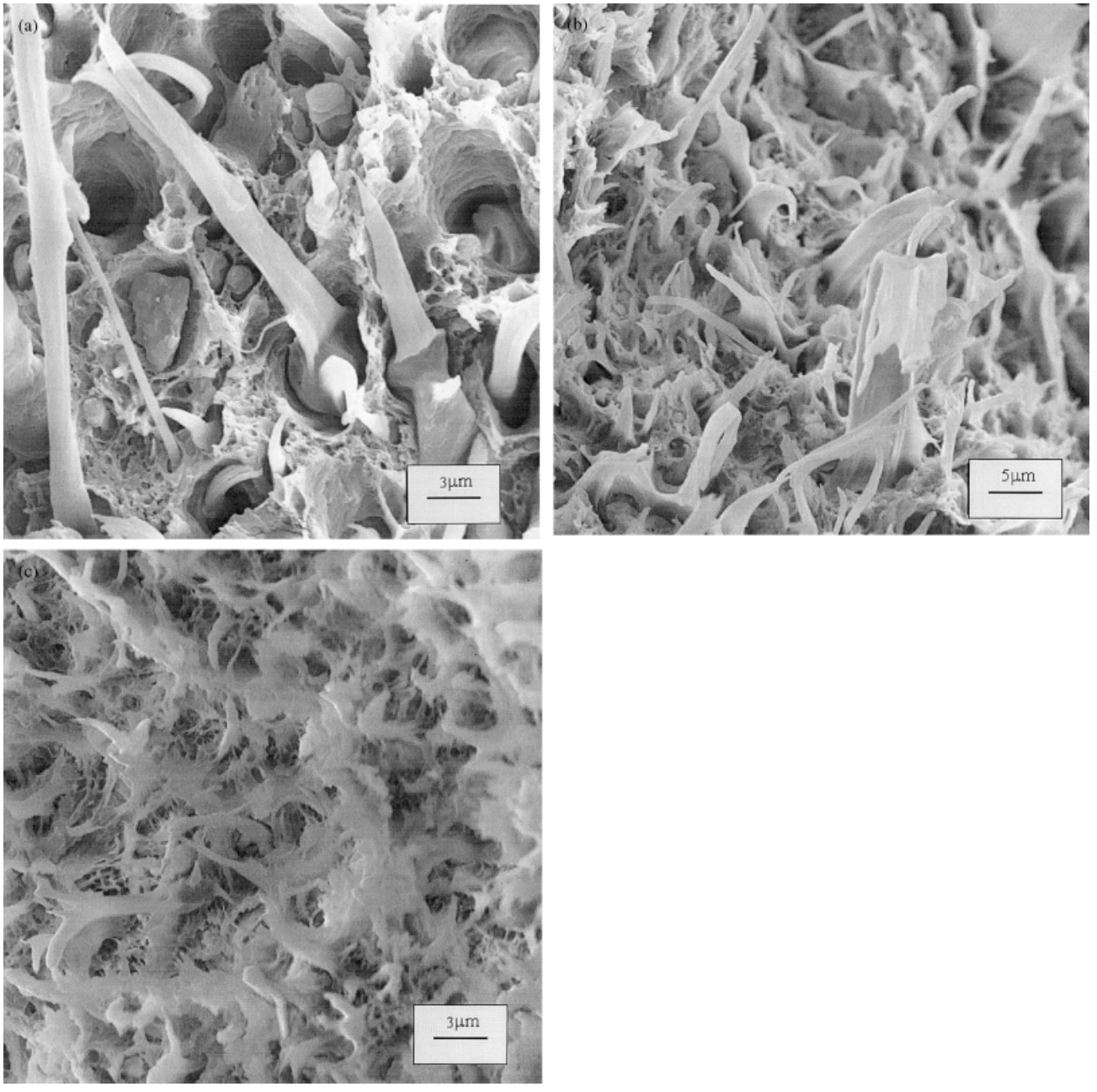

Figure 8 SEM micrographs of the fracture surface of *J*-integral specimens of ABS/PET blends. (a) ABS/PET 67/33 blend, (b) ABS/PET/PC 60/30/10 blend, and (c) ABS/PET/PC/EXL3300 55/27/9/9 blend.

These fibrils elongate to several times their original length before breaking. As a result, the fibrils bridge across the crack and in a sense stabilize the crack propagation, zone B. Upon further deformation of the specimen, the crack propagates into the ABS phase, and the XP fibrils elongate to their ultimate strain and eventually break, leaving the fibrillar morphology in the fracture surface, zone A. Figure 8(a) clearly indicates the deformation of the fibrils, as there are both fibrils and hollow spaces close to the fibrils being pulled out.

The formation of the fibrils contributes to the slow crack propagation toughness. Extra energy absorption is related to

- The pulling out of XP fibrils from the ABS.
- The stabilization of the crack due to the bridging effect of the fibrils across the crack tip.
- The large deformation of fibrils, perhaps several times their original length.

Since many polymer products are subjected to moderate deformation rates, this toughening mechanism has potentially a practical importance. Fiber bridging is regarded as an important toughening mechanism in fibre-reinforced composite materials, and in this case the semicrystalline polymers can in a sense be regarded as a reinforcement of the ABS.

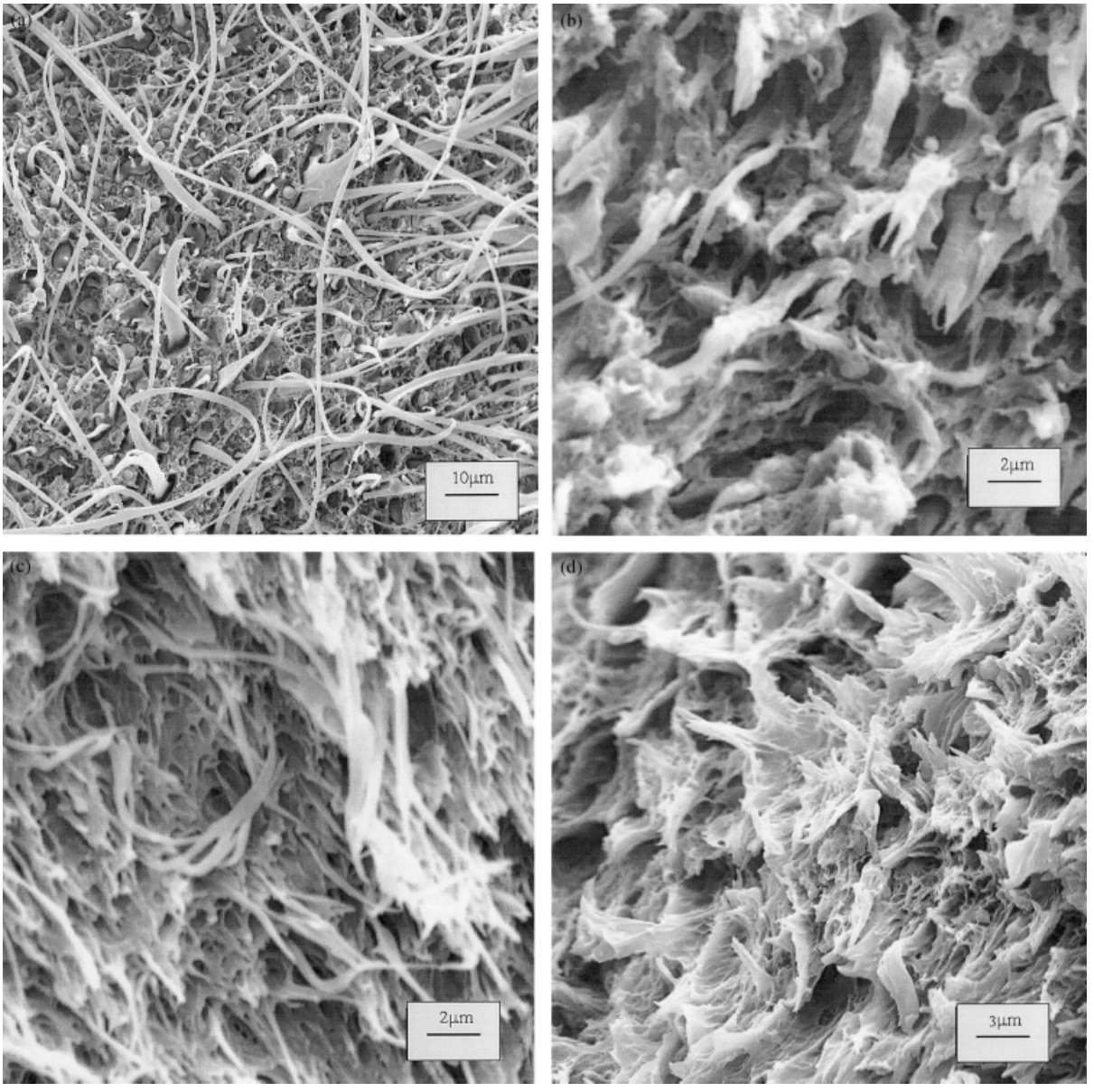

Figure 9 SEM micrographs of the fracture surfaces of *J*-integral specimens of ABS/PBT blends. (a) ABS/PBT 67/33, (b) ABS/PBT/PC/EXL3300 55/27/9/9, (c) ABS/PBT/SMA25/EXL3300 61/27/3/9, and (d) ABS/PBT/PC/EXL3300 45/23/23/9.

On the other hand, fast deformation of the specimens (i.e., during an impact test) and the corresponding fracture do not involve these processes. In this case, the crack simply propagates through the continuous XP phase and the fracture surface has the appearance of a blend with a matrix/dispersed phase morphology. This is the reason why some ABS/XP blends do not display very high impact strengths, but fairly good J_C values and high crack resistance as measured by the *J-R* curve. For the ABS/XP blends with a higher impact strength, the XP phase is more finely dispersed in the ABS matrix. Obviously, the compatibilization agent is important in that case. Although fibril formation does not take place at a high deformation rate (impact), other toughening mecha-

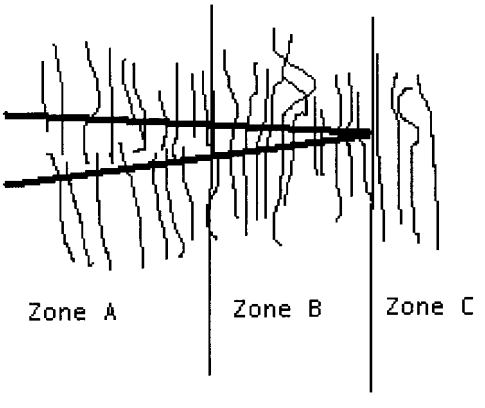

Figure 10 Scheme of fibril formation during slow crack propagation.

nisms, such as void formation, shear yielding, and crazing are operative. In this case, the particle size and the dispersion of the XP phase influence the impact fracture properties at high deformation rates. Since processes like pulling out, elongation of fibrils, and bridging do not take place at high rates, the impact strengths of the ABS/XP blends are in general not very impressive. However, if there is a semicrystalline polymer that has a very low ductile/brittle transition temperature, the blend of this polymer with ABS might exhibit a high impact strength, and fibril formation might occur at higher deformation rates.

CONCLUSIONS

1. The morphology studies indicated that the reactive compatibilizers with maleic anhydride and epoxy functional groups can significantly reduce the interfacial tension between SAN and PA, PBT, and PET. The mechanical properties of ABS/PA, ABS/PBT, and ABS/PET blends can thus be upgraded with small amounts of such compatibilizers and core–shell impact modifiers. The effect of compatibilizers on the morphology will also be further discussed in a future work.
2. Blends of ABS and semicrystalline plastics exhibited a co-continuous structure at a certain composition. The solidification temperatures of PA, PET, and PBT were in this case rather close to the processing temperature. This could provide an explanation of the development of the co-continuous structures in the ABS/XP blends. The semicrystalline polymers are believed to exhibit strain hardening during the processing, when subjected to elongational flow.
3. Due to the differences in deformation rate and deformation mechanism, toughness characterized with the Charpy impact and with the *J*-integral method often does not exhibit the same trend. The fracture mechanism differs at high and low deformation rates and the corresponding fracture surfaces of a polymer blend appear to be quite dissimilar. The formation of fibrils contributed to the higher energy absorption during the *J*-integral test at a low deformation rate.

The authors wish to express their appreciation for financial support from the Foundation for Strategic Environmental Research (MISTRA). We are grateful to Bayer Sverige AB, BASF AB, and AB Svenska Shell for providing materials. Thanks are also extended to Dr. J. A. Bristow for the linguistic revision of the manuscript.

References

1. Liu, X.; Bertilsson, H. Polym Recycl 1997/1998, 3, 107–117.
2. Triacca, V. J.; Ziaee, S.; Barlow, J. W.; Keskkula, H.; Paul, D. R. Polymer 1991, 32, 1401–1413.
3. Majumdar, B.; Keskkula, H.; Paul, D. R. Polymer 1994, 35, 4263–4279.
4. Majumdar, B.; Keskkula, H.; Paul, D. R. Polymer 1994, 35, 3164–3172.
5. Misra, A.; Sawhney, G.; Kumar, R. A. J Appl Polym Sci 1993, 50, 1179–1186.
6. Kim, B. K.; Lee, Y. M. Polymer 1993, 34, 2075–2080.
7. Kudva, R. A.; Keskkula H.; Paul, D. R. Polymer 1998, 39, 2447–2460.
8. Kalfoglou, N. K.; Skafidas, D. S.; Kallitsis, J. K. Polymer 1996, 37, 3387–3395.
9. Fox, B.; Moad, G.; Van Diepen, G.; Willing, I.; Cook, W. D. Polymer 1997, 38, 3035–3043.
10. Cook, W. D.; Zhang, T.; Moad, G.; Van Diepen, G.; Cser, F.; Fox, B; Oshea, M. J Appl Polym Sci 1996, 62, 1699–1708.
11. Cook, W. D.; Zhang, T.; Moad, G.; Van Diepen, G.; Cser, F.; Fox, B.; Mccarthy, L. J Appl Polym Sci 1996, 62, 1709–1714.
12. Hage, E.; Hale, W.; Keskkula, H.; Paul, D. R. Polymer 1997, 38, 3237–3250.
13. Basu, D.; Banerjee, A. J Appl Polym Sci 1997, 64, 1485–1487.
14. Lee, P.; Kuo, W.; Chang, F. Polymer 1994, 35, 5641–5650.
15. Hale, W.; Keskkula, H.; Paul, D. R. Polymer 1999, 40, 365–377.
16. Hale, W.; Keskkula, H.; Paul, D. R. Polymer 1999, 40, 3353–3365.
17. Hale, W.; Lee, J. H.; Keskkula, H.; Paul, D. R. Polymer 1999, 40, 3621–3629.
18. Hale, W.; Keskkula, H.; Paul, D. R. Polymer 1999, 40, 3665–3676.
19. Utracki, L. A., Ed. Encyclopaedic Dictionary of Commercial Polymer Blends; ChemTec Publishing, 1994.
20. Huang, D. D. Plastic Eng 1996, June, 37–39.
21. Williams, J. G. Fracture Mechanics of Polymers; Ellis Horwood: Chichester, UK, 1984.
22. Lu, M.; Keskkula, H.; Paul, D. R. Polymer 1993, 34, 1874–1885.
23. Mannas-Zloczower, I.; Tadmer, Z., Eds. Mixing and Compounding of Polymers, Theory and Practice; Hanser Publishers, 1994
24. Utracki, L. A. Polymer Alloys and Blends; Thermodynamics and Rheology, Hanser Publishers, 1989.
25. Champagne, M.; Mumoulin, M.; Utracki, L. Polym Eng Sci 1996, 36, 1636–1646.
26. Tjong, S. C.; Ke, Y. C. Eur Polym J 1998, 34, 1565–1570.
27. Robeson, L.; Axelrod, R. Polym Prep 1992, 32:2, 620–621.
28. Tsebrenko, M.; Yudin, A.; Ablazova, T. Polymer 1976, 17, 831–834.
29. Jang, S. H.; Kim, B. S. Polym Eng Sci 1995, 35, 528–537.
30. Kwon, S. K.; Chung, I. J Polym Eng Sci 1995, 35, 1137–1144.